

# Automatic Detection of Concrete Surface Defects Using Deep Learning and Laser Ultrasonic Visualization Testing

Takahiro Saitoh<sup>1</sup>, Syumpei Ohyama<sup>2</sup>, Tsyoshi Kato<sup>3</sup>, and Sohichi Hirose<sup>4</sup>

<sup>1,2</sup> *Department of Civil and Environmental Engineering, Gunma University, 1-5-1, Tenjin, Kiryu, Gunma, 376-8515, Japan*  
t-saitoh@gunma-u.ac.jp  
t190c025@gunma-u.ac.jp

<sup>3</sup> *Department of Informatics, Gunma University, 4-2, Aramaki, Maebashi, Gunma, 371-0044, Japan*  
katotsu.cs@gunma-u.ac.jp

<sup>3</sup> *Department of Civil and Environmental Engineering, Tokyo Institute of Technology,  
2-12-1, Ookayama, Merugo, Tokyo, 152-8552, Japan*  
shirose@cv.titech.ac.jp

## ABSTRACT

In recent years, nondestructive testing of civil engineering structures has become increasingly important. Ultrasonic testing is one of nondestructive inspection methods for civil structures. However, the inspection of civil engineering structures takes much time because of the extensive scope of the inspection. Moreover, in the field of nondestructive testing, there are also concerns about a future shortage of inspectors, so that an innovative effective nondestructive method need to be developed. This study proposes using deep learning for laser ultrasonic visualization testing. The effectiveness of the proposed method is confirmed by applying it to a concrete structure with a surface defect.

## 1. INTRODUCTION

Nondestructive testing has become increasingly important for civil and mechanical engineering structures in recent years. The ultrasonic method is the most widely used nondestructive evaluation method in the field (Rose, 2008)(Schmerr, 1998). The presence, absence, and location of defects in the ultrasonic nondestructive evaluation method are determined by checking for scattered waves. However, it is difficult to determine the location of defects from only a simple A-scope waveform. Especially for concrete materials, this determination is more difficult because the received waveform contains a lot of noise.

There exists a method called Laser Ultrasonic Visualization

Testing (LUVT) (Takatsubo et al., 2008) that can quickly determine the presence or absence of defects at a glance. LUVT can visualize ultrasonic wave propagation on the laser irradiated surface, as will be shown later. The greatest advantage of LUVT is that it can easily determine the presence and location of defects from ultrasonic visualization results, even if the inspector is not familiar with nondestructive testing. For example, Yashiro et al. (Yashiro, Toyama, Takatsubo, & Shiraiishi, 2010) used LUVT to visualize ultrasonic wave propagation in welds. Saitoh et al.(Saitoh, Mori, Ooashi, & Nakahata, 2019) estimate elastic constants of CFRP (Carbon Fiber Reinforced Plastic) with the acoustic anisotropy from time-domain ultrasonic wave propagation images generated by using LUVT. While LUVT has been applied to metallic and anisotropic materials like CFRP, its application to concrete has been limited. The reason for this is that ultrasonic wave propagation in concrete is extremely complicated by multiple scattering due to material inhomogeneity.

On the other hand, the use of artificial intelligence (AI) has attracted attention as a means of automating non-destructive inspections. AI is being considered in nondestructive testing to reduce the workload of inspectors. Meng et al. (Meng, Chua, Wouterson, & Ong, 2017) used a deep convolutional neural network to identify a defect from ultrasonic waveforms. Saitoh et al. (Saitoh, Kato, & Hirose, 2021) utilized deep learning to identify the presence or absence, and type of a defect in images obtained by the time-domain boundary element method (Saitoh, Hirose, Fukui, & Ishida, 2007) that are equivalent to those obtained by LUVT. On the other hand, Nakajima et al.(Nakajima, SAITOH, & KATO, 2022) predicted the presence or absence of defects in images by performing deep CNN (Convolutional Neural Network) on im-

Takahiro SAITOH et al. This is an open-access article distributed under the terms of the Creative Commons Attribution 3.0 United States License, which permits unrestricted use, distribution, and reproduction in any medium, provided the original author and source are credited.

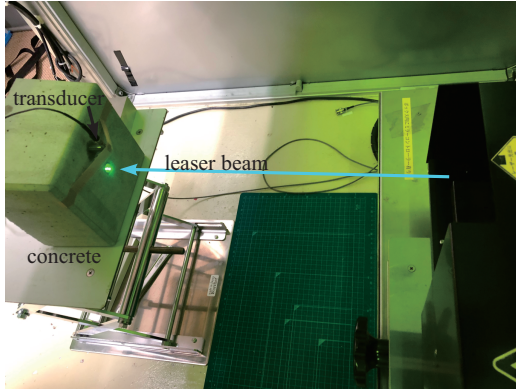


Figure 1. LUVT experimental setup for a concrete specimen.

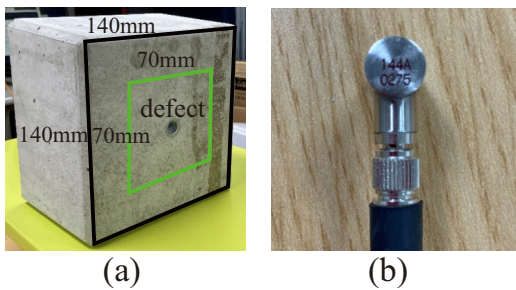


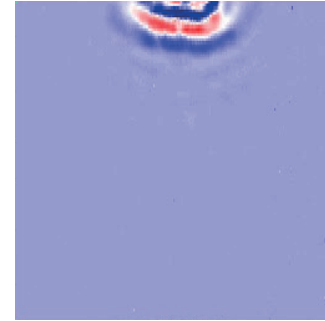
Figure 2. A concrete specimen and the sensor used in this study.

age data obtained by LUVT on actual isotropic homogeneous materials. While deep learning has been applied to determine the presence or absence of defects in LUVT images of isotropic homogeneous materials, it has not been widely used for materials with strong heterogeneity, such as concrete.

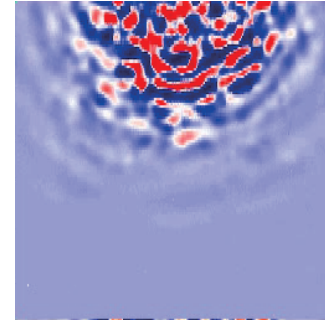
Therefore, this study aims to use deep learning to determine the presence or absence of defects in LUVT images of concrete materials, building on previous research. In the following, we first describe the experimental conditions and other aspects of LUVT conducted in this study. Next, we present examples of ultrasonic wave propagation images of concrete material surfaces obtained by LUVT. After a brief description of deep learning, we present the results of determining the presence or absence of defects in actual concrete material LUVT images. Finally, we summarize the conclusions and future issues.

## 2. LUVT SETUP

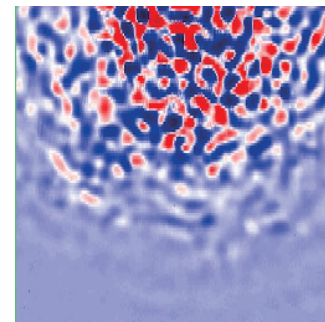
LUVT experimental condition is introduced in this section. Fig. 1 shows the practical LUVT situation for a concrete specimen in this research. A laser emitted from the right side in Fig. 1 is irradiated onto the front surface of the concrete specimen. The laser ultrasonic waves are excited from the laser irradiation spots, they propagate and some of them are received by an AE sensor. In this work, an AE sensor with



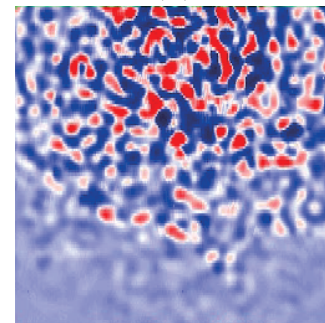
(a)



(b)



(c)



(d)

Figure 3. Time-variations of laser ultrasonic wave propagation on the surface of the concrete specimen without a defect.

the 144KHz central frequency is utilized as shown in Fig. 2. The surface geometry of the concrete specimen is about 140 mm × 140 mm and this concrete specimen has a pene-

trate cavity with diameter  $\approx 10$  mm. This laser ultrasonic wave reception process is repeated for many irradiation spots, according to the laser scan. Then, using the reciprocity theorem (Achenbach, 2004), the laser irradiation point and the receiving point can be swapped to obtain a waveform as if ultrasonic waves were transmitted from the receiving point. The laser irradiation points are taken within the front face of the concrete specimen, covering an area of approximately  $70 \text{ mm} \times 70 \text{ mm}$ , shown by the green line in Fig. 2(a). In this study, the laser pitch spacing  $\Delta x$  and  $\Delta y$  in the horizontal and vertical directions are set as  $\Delta x = 0.237 \text{ mm}$  and  $\Delta y = 0.582 \text{ mm}$ , respectively. The laser irradiation points  $N_x$  and  $N_y$  for each direction are  $N_x = 295$  and  $N_y = 120$ , respectively. The sampling rate in this measurement experiment is 12.5 MHz.

A number of such LUVT experiments are carried out to prepare a number of ultrasonic wave propagation images of the surface of the concrete specimen, as shown in Fig. 1. The ultrasonic wave propagation images obtained here are used as training and test data for the deep learning described in Section 4.

### 3. VISUALIZATION OF ULTRASONIC WAVES ON CONCRETE SURFACE

In general, a concrete is inhomogeneous material with aggregates. The multiple scattering is generated by the interaction between an incident wave and aggregates. Therefore, the incident wave with a small wavelength, which is comparable to the size of aggregates, is not typically used due to the multiple scattering it induces. In this work, the larger defect than general aggregate size is considered.

Figs. 3 and 4 show examples of LUVT results for a concrete specimen without and with a defect, respectively. In the case with a defect, the defect is located slightly above the centre. In the process of image processing, a 500KHz bandpass filter is used. Focusing on the case with a defect in Fig. 3, the incident wave from the top center travels to lower surface along with the multiple scattering. As seen in Fig. 3, the ultrasonic wave propagation and scattering phenomena in concrete materials are very complicated. On the other hand, we examine the case with a defect as shown in Fig. 4. In Fig. 4(a), the incident wave is transmitted. Although the experimental conditions for the LUVT are the same as those for the defect-free case, it can be observed that the ultrasonic wave propagation differs from that shown in Fig. 3 due to the differences in the test specimens and the appearance of the aggregate distribution inside the concrete. In Fig. 4(b), it can be seen that the incident wave reaches the vicinity of the defect. Because the incident wave cannot propagate inside the cavity, it can be observed propagating around it. In addition, as shown in Figs. 4(c) and (d), the incident wave propagates with repeated multiple scattering between aggregates.

From Figs. 3 and 4, it is clearly difficult to identify a defect

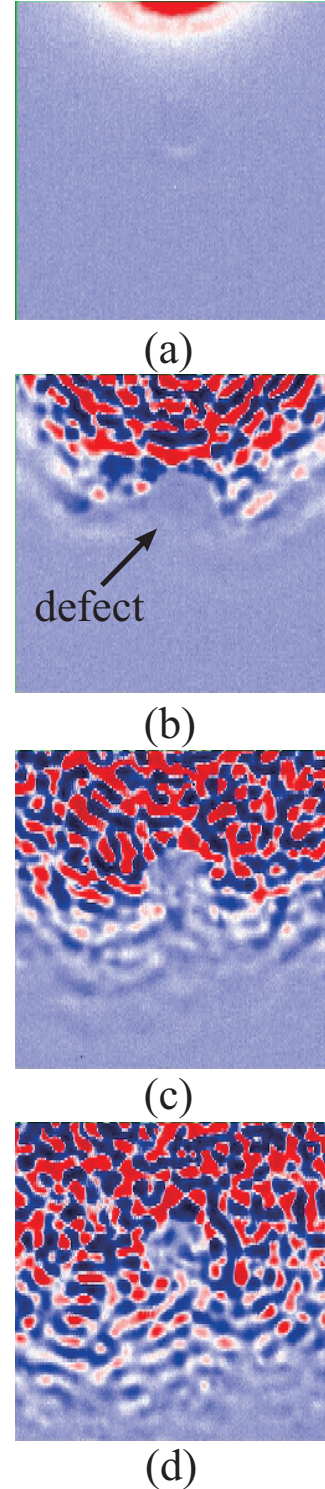


Figure 4. Time-variations of laser ultrasonic wave propagation on the surface of the concrete specimen with a defect.

when the size of the defect is comparable to that of the aggregate. Thus, the limited detectability of defect size in concrete can be observed. Note that, theoretically, the ultrasonic waves

do not propagate inside the defect. However, due to noise in the laser measurement, it appears that a slight ultrasonic wave propagation occurs inside the cavity in Figs. 4(c) and (d).

Now, the inspector must visually determine the presence, location, and size of defects based on the images obtained from the LUVT test (or ultrasonic wave propagation movies generated from a group of images) as shown in Figs. 3 and 4. If machines are capable of making these visual judgments, not only could the workload of inspectors be reduced, but inspections could be conducted more efficiently. Future robotic inspections will be possible if machines can automatically determine the presence or absence of defects. Therefore, in the following sections, an attempt is made to use deep learning to identify the presence or absence of defects in the LUVT images as shown in Figs. 3 and 4.

#### 4. DEEP LEARNING

In general, CNN is highly effective when the training data are images. A CNN-trained AI can detect features in images by itself. Therefore, in this study, the deep learning (Chollet, 2017) is used to determine the presence or absence of a defect in images as shown in Figs. 3 and 4. In deep CNN, the weights in the neural network are determined using the back propagation method. As CNN has been thoroughly examined in many literatures, we will not go into its detail in this paper.

The CNN architecture used in this analysis can be seen in Table 1. This study focuses on determining the presence or absence of defects only. In other words, the problem to be solved is a two-classification problem. Therefore, the structure of the deep network is relatively simple, as shown in Table 1. As shown in this Table, the input image size is  $224 \times 224$  and the presence or absence of a defect is determined in the output of this CNN. The sparse categorical crossentropy is used for the loss function and Adam for the optimiser. The softmax function was used for the activation function in the output layer and the ReLU function for the rest. The ReLU function is an output function with an output of zero if the input value is less than or equal to zero and as is if the input value is greater than zero. As hyperparameters, a learning rate of 0.001 and a weight decay for regularisation of 0.0001 are given. A hold-out method was used for training, where 80% of the total data was used for training and the remaining 20% was used for validation. The mini-batch size was 32 and the training epoch was 32. The total number of LUVT images prepared was 14856. Nvidia GPU Geforce3090RTX with 24GB memory is utilized for CNN calculations.

#### 5. DEEP LEARNING RESULTS

Some deep learning results are shown in this section.

Table 1. CNN architecture used in the section 5.

| Layer(type)                | Output Shape      | Param.  |
|----------------------------|-------------------|---------|
| Conv2D                     | (None,224,224,64) | 640     |
| Conv2D-1                   | (None,224,224,32) | 18464   |
| MaxPool.2D                 | (None,112,112,32) | 0       |
| Conv2D-2                   | (None,112,112,16) | 4624    |
| MaxPool.2D-1               | (None,56,56,16)   | 0       |
| Dropout                    | (None,56,56,16)   | 0       |
| Flatten                    | (None, 50176)     | 0       |
| Dense                      | (None, 128)       | 6422656 |
| Dense-1                    | (None, 2)         | 258     |
| Total Params.: 6446642     |                   |         |
| Trainable Params.: 6446642 |                   |         |
| Non-trainable Params:0     |                   |         |

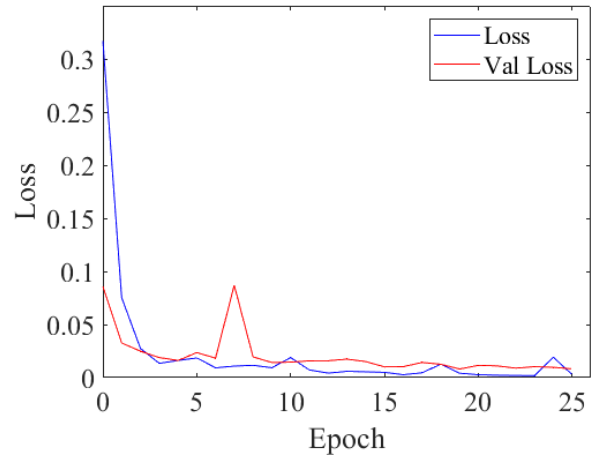


Figure 5. Trends in losses to learning epochs.

##### 5.1. Learning results

First, the deep learning for the neural network architecture in Table 1 is carried out for the LUVT images as shown in Figs. 3 and 4. Fig. 5 and 6 show the loss and accuracy results for the learning epochs, respectively. In this calculation, the training and validation schemes are early finished using early-stopping. In these figures, the solid blue and red lines indicate the results for training and validation respectively. The loss described here is a measure of the certainty of the deep learning model that is being trained. On the other hand, it should be noted that accuracy is a measure of whether a given image has been classified correctly, and that accidental correct decisions may be included in this accuracy.

The results in Fig. 5 show that the value of the loss decreases as the learning epoch progresses. On the other hand, as shown in Fig. 6, the corresponding accuracy values are higher. From the above, it can be concluded that the deep learning model was generally created correctly.

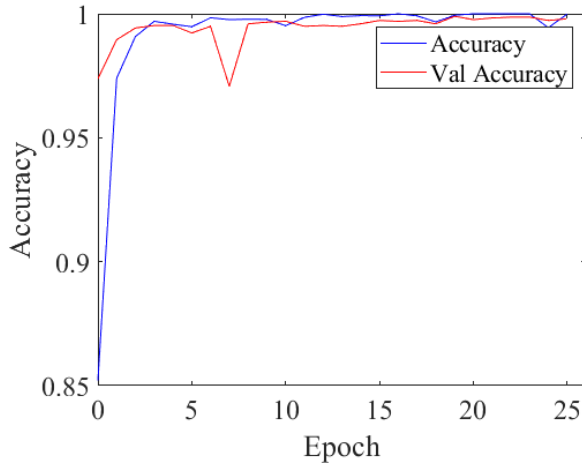


Figure 6. Trends in accuracy to learning epochs.

## 5.2. Test for unlearning LUVT data

The deep learning model created in this study is then tested with a series of untrained time-series image data to evaluate its ability to correctly determine the presence or absence of defects. The number of unknown time-series image data used in this test is 660. At approximately the 400 time step, the presence or absence of a defect can be visually confirmed by an inspector. Fig. 7 shows the time steps of the time series images and the probability of the presence of a defect predicted by the deep learning model. As shown in Fig. 7, we can observe that the probability of the defect presence is correctly predicted as zero up to around 400 time steps. After that, the probability increases, indicating that the presence of a defect is generally predicted correctly, except for some sections.

## 5.3. Confusion matrix

As mentioned in the previous section, the predicted outcomes may include those that could have been predicted by chance. Therefore, the confusion matrix with TP(true positive), FP(false positive), FN(false negative) and TN(true negative) is investigated in this section. Table 2 shows the confusion matrix for the test results performed on a set of untrained time series images. In Table 2, "Actual" indicates whether a defect is present (defect) or not (no defect), while "Predicted" indicates the result predicted by the AI for a given image (defect or no defect). As shown in Table 2, there were 148 cases where a defect-free image was incorrectly identified as having a defect. However, the AI misclassified images containing defects as defect-free in only 6 cases. In non-destructive testing, overlooking defects can lead to critical accidents. In that sense, a small FN (false negative), as shown in Table 2, can be considered an acceptable result.

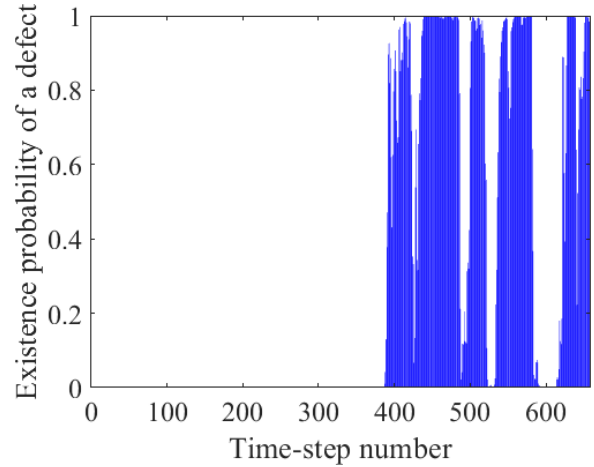


Figure 7. Relation between time-step number and existence probability of a defect.

Table 2. Confusion Matrix

|        |           | Predicted |           |
|--------|-----------|-----------|-----------|
|        |           | defect    | no defect |
| Actual | defect    | 44(TP)    | 6(FN)     |
|        | no defect | 148(FP)   | 462(TN)   |

## 6. CONCLUSION

In this paper, we presented our approach for automatic defect detection in concrete materials using deep learning and LUVT. Our results demonstrated that the deep learning-based AI can accurately detect the presence or absence of a defect in concrete materials with an accuracy of over 75%. However, our results show that the probability of defect detection by the deep learning-based AI is not always sufficient. The factors that make LUVT experiments challenging in concrete are the multiple scattering of ultrasonic waves by aggregates and the rapid attenuation of them compared to homogeneous metals. Indeed, when the target material for LUVT experiments is steel or aluminum, it is relatively easy to visually confirm the generation of scattered waves. On the other hand, it can often be challenging to visually confirm even the scattered waves caused by a defect, and making it difficult to create accurate and reliable training data.

Therefore, in the future, to improve the accuracy of the deep learning model, additional LUVT experiments are planned to be conducted to increase the training data as shown in Figs. 3 and 4. However, preparing a large number of concrete specimens, creating various artificial defects, and conducting LUVT experiments on them require significant effort and cost. To overcome the difficulty, we will explore the use of transfer learning with simulated image data generated using numerical methods such as the finite difference time-domain (FDTD) and finite element method (FEM). Furthermore, we plan to use GAN(Goodfellow et al., 2014) to detect a defect in

LUVT images of concrete materials containing aggregates. In this study, human annotators are responsible for labeling the presence or absence of a surface defect in the training data. However, determining the presence of a defect in LUVT images for concrete materials proves to be challenging for human observers. Consequently, creating a learning model capable of handling such noisy training data (Song, Kim, Park, Shin, & Lee, 2022) is also future research challenge.

#### ACKNOWLEDGMENT

This work was supported by “Joint Usage/Research Center for Interdisciplinary Large-scale Information Infrastructures”, and “High Performance Computing Infrastructure” in Japan (Project ID: jh220033 and jh230036). Additionally, funding from JSPS KAKENHI (21K0423100) and the SECOM Science and Technology Foundation supported this work.

#### REFERENCES

- Achenbach, J. D. (2004). *Reciprocity in elastodynamics*. Cambridge University Press.
- Chollet, F. (2017). *Deep learning with python*. Manning Publications.
- Goodfellow, I., Pouget-Abadie, J., Mirza, M., Xu, B., Warde-Farley, D., Ozair, S., ... Bengio, Y. (2014). Generative adversarial nets. *Advances in neural information processing systems*, 2672-2680. doi: <https://doi.org/10.48550/arXiv.1406.2661>
- Meng, M., Chua, Y. J., Wouterson, E., & Ong, C. P. K. (2017). Ultrasonic signal classification and imaging system for composite materials via deep convolutional neural networks. *Neurocomputing*, 257, 128-135. doi: <https://doi.org/10.1016/j.neucom.2016.11.066>
- Nakajima, M., SAITOH, T., & KATO, T. (2022). A study on deep cnn structures for defect detection from laser ultrasonic visualization testing images. *Artificial Intelligence and Data Science*, 3(J2), 916-924 (in Japanese). doi: 10.1006/jabr.1994.1114
- Rose, J. L. (2008). *Ultrasonic waves in solid media*. Cambridge University Press.
- Saitoh, T., Hirose, S., Fukui, T., & Ishida, T. (2007). Development of a time-domain fast multipole beam based on the operational quadrature method in a wave propagation problem. *Advances in Boundary Element Techniques VIII*, 355-360.
- Saitoh, T., Kato, T., & Hirose, S. (2021). Deep learning for scattered waves obtained by time-domain boundary element method and an attempt to classify defect types. *Journal of JSNDI*, 70(7), 272-279 (in Japanese). doi: 10.1006/jabr.1994.1114
- Saitoh, T., Mori, A., Ooashi, K., & Nakahata, K. (2019). Development of a new dynamic elastic constant estimation method for frp and its validation using the fdtd

method. *Insight- Non-Destructive Testing and Condition Monitoring*, 61(3), 162-165.

- Schmerr, L. W. (1998). *Fundamentals of ultrasonic nondestructive evaluation*. Plenum Press.
- Song, H., Kim, M., Park, D., Shin, Y., & Lee, J.-G. (2022). *Learning from noisy labels with deep neural networks: A survey*. doi: <https://doi.org/10.48550/arXiv.2007.08199>
- Takatsubo, J., Miyauchi, M., Tsuda, H., Toyama, N., Urabe, K., & Wang, B. (2008). Generation laser scanning method for visualizing ultrasonic waves propagating on a 3-d object. In *1st international symposium on laser ultrasonics: Science, technology and applications*.
- Yashiro, S., Toyama, N., Takatsubo, J., & Shiraishi, T. (2010). Laser-generation based imaging of ultrasonic wave propagation on welded steel plates and its application to defect detection. *Materials Transaction*, 51(11), 2069-2075. doi: <https://doi.org/10.2320/matertrans.M2010204>

#### BIOGRAPHIES

**T. Saitoh** Takahiro SAITOH is an Associate Professor at Gunma University, Japan. He received his Doctor of Engineering degree from the Department of Mechanical and Environmental Informatics at Tokyo Institute of Technology in 2006. Previously, he worked as a Japan Society for the Promotion of Science Assistant Professor at the University of Fukui, Japan. His research areas include applied mechanics, computational mechanics, and ultrasonic nondestructive evaluation. He has received several awards, including the Best Paper Award from the Japan Society for Computational Engineering Mechanics (JSCES) in 2008, the Best Paper Award from the Japan Society for Applied Mechanics (JSAM) in 2013, and the Best Paper Award from the Japan Society for Non-Destructive Inspection in 2022. He is also a member of the Japan Society for Applied Mechanics (JSAM) Committee, the Japan Society for Computational Science (JAS-COME), and the Japan Society for Non-Destructive Inspection (JSNDI).

**T. Kato** Tsuyoshi KATO is a Professor at Gunma University, Japan. He received his Doctor of Engineering degree from Tohoku University in 2003. He is a member of JSNDI and the Information Processing Society of Japan (IPSJ). His current scientific interests include pattern recognition and non-destructive testing.

**S. Hirose** Sohichi HIROSE is a Professor Emeritus of Tokyo Institute of Technology, Japan. In 1987, he received his Doctor of Engineering degree from Kyoto University. He is a member of both JASCOME and JSNDI. He received several awards, including the best paper award of JSCES in 2008, the Best Paper Award from JSAM in 2013, and the Best Paper Award from JSNDI in 2022. His research interests include ultrasonic nondestructive evaluation and inverse problems.